Ceramics-Silikáty 66 (4), 498-507 (2022)
www.ceramics-silikaty.cz doi: 10.13168/cs.2022.0046

EFFECT OF BORON IMPURITIES ON THE PROPERTIES OF MAGNESIUM OXYCHLORIDE CEMENT

YONG ZHANG*, #CHENYOU WU*, **, LEI HUANG*, **, XIAOYUAN ZHANG*

*School of Civil Engineering, Qinghai University, Xining 810016, PR China
**Qinghai Provincial Key Laboratory of Energy-saving Building Materials and Engineering Safety, Xining 810016, PR China

#E-mail: wuchengyou86@163.com

Submitted August 8, 2022; accepted September 14, 2022

Keywords: Magnesium oxychloride cement, Magnesium oxide, Boron impurity, 5·1·8 phase, Compressive strength

Magnesium hydroxide was used as a precursor to magnesium oxide (MgO). Magnesium oxide cement (MOC) was calcined at different temperatures to obtain MgO with different activities in the presence of 0 %, 3 % and 5 % boric acid (H_3BO_3). Cement hydration, which is an exothermic reaction, determines the phase composition and pore structure. In addition, the effect of boron, a common impurity occurring in Salt Lake, on the MOC compressive strength was explored. H_3BO_3 has a negative effect on the MOC strength, and slows the MOC condensation and hardening. However, the presence of H_3BO_3 impurities does not change the hydration phase composition of MOC, because the specific surface area of MgO increases after calcination at 700 °C. As a result, the grain size decreases and the internal defects increase, which affects the phase number and morphology (5·1·8 phase) and, thereby, determines the compressive strength of the MOC. In addition, after calcination at 1000 °C, the adjacent MgO is continuously sintered. The large amount of rough magnesium borate generated adheres to the surface of MgO, which inhibits the hydration reaction of the MgO and the formation of the 5·1·8 phase and, thus, reduces the MOC compressive strength.

INTRODUCTION

Magnesium oxychloride cement (MOC) is an air-hardening gel manufactured from lightly-burnt magnesium oxide (MgO), magnesium chloride ($MgCl_2$), and water (H_2O). It was first discovered by Sorel in 1867 [1]. Compared with traditional Portland cement, MOC hardens and sets rapidly and exhibits excellent bonding properties [2-4]. Some organic or inorganic aggregates show strong adhesion and good resistance to wear and corrosion. The wear resistance of magnesium cement is three-fold higher than that of ordinary Portland cement. Furthermore, it shows good heat insulation and flame retardance due to the use of non-flammable raw materials, MgO and $MgCl_2$ [5-6]. The strength of the hydration products in MOC is mainly attributed to the crystallisation of the 5·1·8 and 3·1·8 phases (Formula 1 and Formula 2). At room temperature, most of them exist in the 5·1·8 phase, and the degree of crystallisation usually determines the compressive strength of MOC. Microscopically, the 5·1·8 phases appear needle-shaped and are affected by different growth spaces and external factors. Occasionally, they appear as granular or fibre-like aggregates intersecting and overlapping with each other into a felt-like porous mesh structure [7-8].

$$5MgO+MgCl_2\cdot 6H_2O+7H_2O\rightarrow 5Mg(OH)_2\cdot MgCl_2\cdot 8H_2O \quad \text{(Phase 5)} \quad (1)$$

$$3MgO+MgCl_2\cdot 6H_2O+5H_2O\rightarrow 3Mg(OH)_2\cdot MgCl_2\cdot 8H_2O \quad \text{(Phase 3)} \quad (2)$$

The raw materials for $MgCl_2$ used in the preparation of MOC-samples are mainly derived from seawater and Salt Lake brine. The $MgCl_2$ derived from the Salt Lake brine constitutes approximately 3.14 billion tonnes, and the seawater $MgCl_2$ reserves amount to 4493 trillion tonnes [9]. However, a mere 300,000 to 500,000 tonnes of $MgCl_2$ are sold each year as a primary product. As a result, a large amount of $MgCl_2$ is directly discharged back to the Salt Lake in the form of halogens, which wastes the resources, pollutes the Salt Lake environment, and causes "magnesium harm" [10]. The active MgO used in the preparation of MOC is primarily derived from calcined magnesite ($MgCO_3$) [11], which is mainly distributed in Liaoning, Shandong and other provinces. Semi-roasted dolomite ($CaCO_3\cdot MgCO_3$) is found almost all over the country; however, calcination reduces the MgO content [12,13]. Due to resource imbalance and the high cost of transportation in the western region of China,

the preparation of MgO from the existing Salt Lake resources has been envisaged to develop the magnesium industry in western China and manufacture MOC [14]. In summary, the Salt Lake resources can be used to prepare MgO raw materials as well as $MgCl_2 \cdot 6H_2O$ to manufacture MOC. Thus, the utilisation of the waste not only reduces the production costs and saves resources, but also resolves the problem of salt pollution and protects the natural environment.

However, when preparing active MgO and $MgCl_2 \cdot 6H_2O$ from the Salt Lake, a large number of impurities in the brine are a challenge that must be overcome [15]. Therefore, it is generally not desirable to excessively remove the impurities from the Salt Lake brine. For example, the excessive loss of boron impurities leads to a free boron state in MgO and $MgCl_2 \cdot 6H_2O$, which, in turn, affects the performance of the MOC. Due to varying forms of boron, it is better to utilise the magnesium resources of the Salt Lake to manufacture the MOC. Therefore, it is essential to investigate the effects of the free boron impurities present in the $MgCl_2 \cdot 6H_2O$ solution on the MOC and the coexistence of boron impurities when calcining MgO. In this study, magnesium hydroxide ($Mg(OH)_2$) was used as the raw material to prepare MgO. The effect of the free boron on the performance of magnesium oxychloride cement was investigated by directly adding boron impurities to the solution. The effect of boron on the crystallisation or activity of MgO during calcination was analysed by incorporating boron impurities into the magnesium hydroxide for co-calcination. The effects of $MgCl_2$ on the coagulation, hardening, and mechanical properties of chlorate cement were studied.

In this study, the compressive strength of the MOC samples was measured according to the GB175-2007 standard at a loading rate of 0.3 $KN \cdot s^{-1}$. The hydration exothermic rate was determined using an isothermal calorimeter (Calmetrix-4000HPC) at a constant temperature of 20 °C. The X-ray diffraction (XRD) spectra were analysed using an X-ray diffractometer (D/max-2500PC) under Cu Kα radiation (λ = 0.15419 nm) and an accelerating voltage. The XRD pattern was obtained by analysing the sample at 30 KV (2θ is in the range of 5 – 70°). The microscopic morphology of the MOC was determined via scanning electron microscopy (SEM, JSM-6610LV). The cement cube specimens were fragmented, and thin slices with relatively flat interiors were selected for SEM observation after gold spraying. The resolution of the SEM was 4.0 nm, and the test voltage was 10 KV. The pore distributions of the MOC were determined using a fully automated mercury pressure meter (Auto PoreIV 9500), an HCT-1 microcomputer differential thermal balance was used for the thermal analysis of the MOC under a nitrogen atmosphere at a test temperature range of 25 °C to 1050 °C.

EXPERIMENTAL

Raw materials

(1) The $Mg(OH)_2$ (AR: 95 %) used in this experiment was supplied by Shanghai McLin Biochemical Technology Co., Ltd.

(2) The boric acid (H_3BO_3) used in this experiment was produced by Sinopharm Chemical Reagent Co., Ltd. The chemical composition of H_3BO_3 is shown in Table 1.

Table 1. Chemical composition of H_3BO_3.

Component	H_3BO_3	Water insoluble	Metal	Sulfate
Mass fraction (wt. %)	≥ 99.8	≤ 0.005	≤ 0.003	≤ 0.001

(3) The $MgCl_2 \cdot 6H_2O$ was ordered from Tianjin Zhiyuan Chemical Reagent Co., Ltd. The chemical composition of $MgCl_2 \cdot 6H_2O$ is shown in Table 2.

Table 2. Chemical composition of $MgCl_2 \cdot 6H_2O$.

Component	$MgCl_2 \cdot 6H_2O$	Water insoluble	Sulfate	pH
Mass fraction (wt. %)	≥ 98.0	≤ 0.005	≤ 0.005	5.0-6.5

(4) The potassium phosphate monobasic (KH_2PO_4) was manufactured by Hongyan Reagent Factory in Hedong District, Tianjin, and its technology index is shown in Table 3.

Table 3. Chemical composition of KH_2PO_4.

Component	KH_2PO_4	Water insoluble	Sulfate	pH
Mass fraction (wt. %)	≥ 99.5	≤ 0.002	≤ 0.003	4.2-4.5

Preparation of active MgO

The analytically pure $Mg(OH)_2$ powder was calcined with 0 %, 3 %, and 5 % H_3BO_3 at a final temperature of 700 ℃ and 1000 ℃. The heating rate was 10 $°C \cdot min^{-1}$ and the holding time was 1 h. The MgO-samples were prepared and labelled 0T7, 3T7, 5T7, 0T10 and 5T10. Figure 1 shows the XRD pattern of the calcined active MgO at the different temperatures. As shown in the figure, MgO was the main phase obtained at the calcination temperature of 700 ℃, with a higher diffraction peak. When the calcination temperature was 1000 ℃, 0T10 was the main phase of MgO. The diffraction peaks of 5T10 are attributed to magnesium borate and MgO.

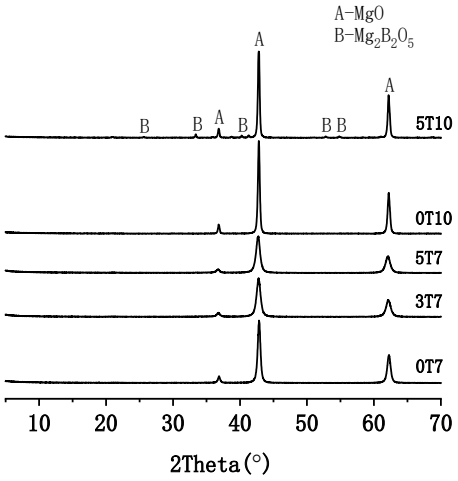

Figure 1. The XRD patterns of the active MgO prepared at the different calcination temperatures.

Figure 2 shows the SEM results of the active MgO samples prepared at different calcination temperatures. As shown in Figure 2a, a large number of tiny pores were formed on the surface of the MgO at the calcination temperature of 700 ℃ in the absence of H_3BO_3. As shown in Figure 2b, in the presence of 5 % H_3BO_3, the micropores on the surface of the MgO are denser due to the presence of H_3BO_3, resulting in a less porous and smooth MgO. As shown in Figures 2c and 2d, when the calcination temperature was 1000 ℃, the amount of H_3BO_3 was 0 %, and a large number of tiny pores were detected on the surface of the MgO. In the presence of 5 % H_3BO_3, the micropores were larger, but the overall structure was relatively tight. Calcination at high temperatures with H_3BO_3 leads to the attachment of large amounts of rough magnesium borate to the surface, and the adjacent MgO is constantly sintered into the larger pores.

Table 4 shows the characterisation of the different active MgO crystals. Calcination at a temperature of 700 ℃ increases the specific surface area following the addition of H_3BO_3, while the grain size decreases, and the degree of crystallisation is reduced. The number of internal defects is increased and the discoloration time of citric acid is prolonged. When the calcination temperature is raised to 1000 ℃, the addition of H_3BO_3

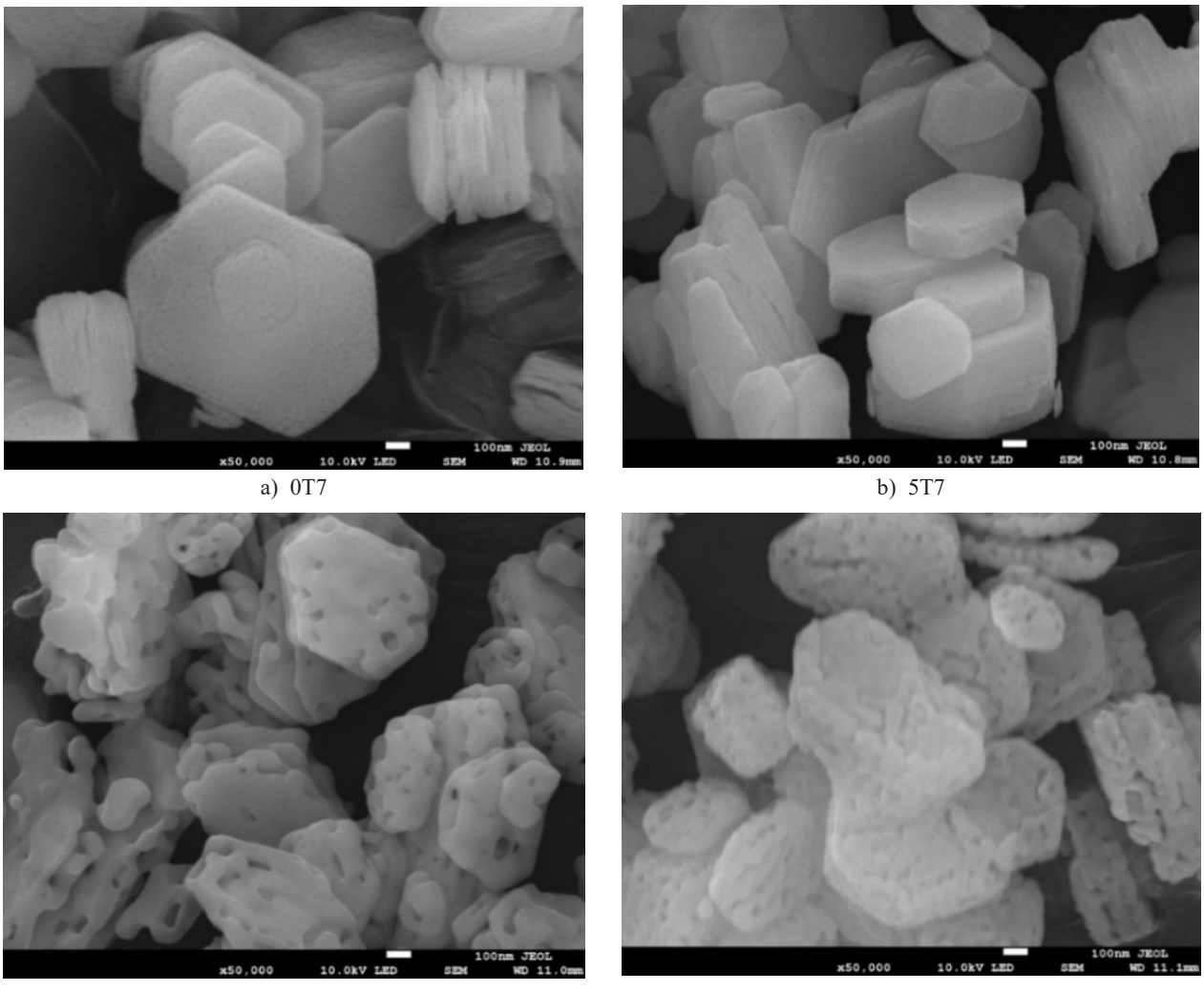

a) 0T7 b) 5T7

c) 0T10 d) 5T10

Figure 2. SEM images of the active MgO prepared at the different calcination temperatures.

Table 4. The related characterisation of the different active MgO

Temperature (°C)	Crystallite dimension (nm)	BET surface area ($m^2 \cdot g^{-1}$)	MgO content (%)	Citric acid discoloration time (s)
0T7	16.80	51.69	95.58	22.69
3T7	11.56	69.50	94.38	24.23
5T7	11.65	78.83	91.28	32.19
T7B3	16.18	51.21	92.80	25.12
T7B5	16.43	51.86	91.03	33.28
0T10	24.07	21.48	100.00	110.36
5T10	33.23	15.27	95.77	143.52
T10B5	24.72	22.72	95.24	112.94

In this table, the grain size of each MgO crystal was calculated according to Scherrer's equation:

$$D = \frac{K \cdot \gamma}{B \cdot \cos\theta} \quad (3)$$

In the formula, D is the average thickness of the grain perpendicular to the crystal surface; K is Scherrer's constant, the numeric value is 0.9; B is the half-width of the diffraction peak; θ denotes the angle of the X-ray diffraction; and γ represents the wavelength of X-ray (0.154056 nm).

The MgO content is determined by calculating the weight loss before and after the magnesium hydroxide calcination. The level of the MgO activity was ascertained based on the discoloration time of the citric acid.

decreases the specific surface area, but decreases the grain size. As a result, the degree of crystallisation is improved while the internal defects are reduced. Furthermore, the discoloration time of the citric acid is prolonged.

Preparation of the cement specimens

The ratio of MgO:$MgCl_2$:H_2O was controlled to 5:1:13. $MgCl_2 \cdot 6H_2O$ was first added to deionised water and continuously stirred to obtain an $MgCl_2$ solution with a mass fraction of 28.88 %. Second, 1 % potassium dihydrogen phosphate was mixed with 0 %, 3 %, and 5 % H_3BO_3 and the $MgCl_2$ solution. Finally, MgO with different crystallisation characteristics at different temperatures was mixed with the $MgCl_2$ solution and stirred to obtain a MOC slurry, which was poured into a steel mould measuring 20 × 20 × 20 mm, and released after 24 h at room temperature and cured to the specified age. The specimen is represented as "X-T, T-X," wherein X represents the impurity ion, and T denotes the temperature. For example, B5T7 represents MgO obtained via co-calcination with 5 % H_3BO_3 at 700 °C. T7B5 represents MgO mixed with 5 % H_3BO_3 obtained at a calcination temperature of 700 °C.

RESULTS AND DISCUSSION

Compressive strength

Figure 3 shows the compressive strength of the MOC doped with H_3BO_3 at different calcination temperatures. As shown in Figure 3a, the strength of the obtained MOC via co-calcination or doping with H_3BO_3 at 700 °C was lower than the compressive strength of the control group and had a more significant impact on the early strength of the MOC. For example, the intensity of the control

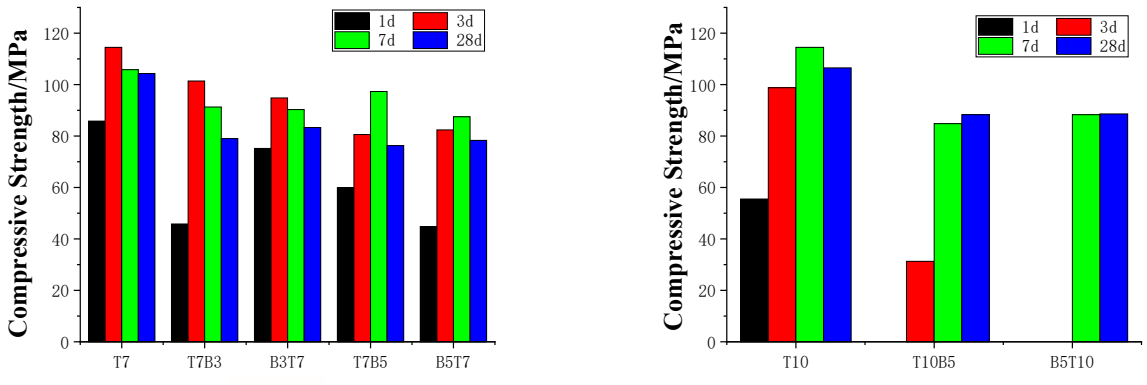

a) 700°C b) 1000 °C

Figure 3. The compressive strength of the MOC doped with H_3BO_3 at the different calcination temperatures.

group T7 after curing for one day was 85.8 MPa, while the intensities of T7B3, B3T7, T7B5, and B5T7 after a similar duration of curing were 45.8 MPa, 75.2 MPa, 59.9 MPa, and 44.8 MPa, respectively. After 28 days (28-d) of curing, the strength of the control group T7 was 104.3 MPa, which was 25.3 MPa, 21 MPa, 28 MPa, and 26 MPa, respectively, compared with T7B3, B3T7, T7B5 and B5T7 doped with H_3BO_3. In the presence of the unchanged water-to-ash ratio, the addition of the H_3BO_3 impurity reduces the concentration of the reactants accordingly. The progressive hydration decreases the contact area between the MgO hydration layer and the $MgCl_2$ solution, thereby inhibiting the formation of the 5·1·8 phase crystal nuclei. As shown in Figure 3b, when the calcination temperature of MgO was 1000 °C, the MOC doped with H_3BO_3 was not completely condensed and hardened due to the slow condensation rate. The compressive strength was less than 0.5 MPa, which was lower than the limits of the pressure detection, so the compressive strength of the boron-containing MOC cured for 1 day was not detected. However, the strength of the control group T10 after 1 day of curing was 55.5 MPa, indicating that the boron impurity generated during the co-incineration has a negative impact on the early strength of the MOC. With the increased duration, the intensity of the MOC continued to increase, and the strength of the control group T10 at 28-d was 106.5 MPa, which was still higher than the strength of the boron-containing MOC. For example, the intensity of T10B5 and B5T10 after 28-d curing decreased by 21 % and 20 %, respectively, compared with the control group. Furthermore, the effect of the H_3BO_3 addition on the early strength of the MOC after the high-temperature calcination of MgO was greater than that of the MOC mixed with H_3BO_3 after the low-temperature calcination. This is because high-temperature calcination generates rough magnesium borate, which adheres to the surface of MgO, thereby delaying the condensation of the MOC. Finally, co-calcination or doping with boron impurities reduced the compressive strength of the MOC.

Hydration characteristics

The hydration of magnesium oxychloride cement is an important factor determining the compressive strength. The course of the hydration can be divided into five stages: initial phase, induction, acceleration, deceleration, and stabilisation [3].

Figure 4 shows the rate of hydration exothermic reaction of MOC at different temperatures and doping levels of H_3BO_3. As shown in Figure 4a, when the calcination temperature was 700 °C, the addition of H_3BO_3 significantly delayed the hydration exothermic rate of the MOC, prolonged the induction phase, and delayed the acceleration period. For example, the start time of the acceleration stage of T7 in the control group was about 3.1 h, while the start times of the acceleration stage of B3T7, B5T7, T7B3 and T7B5 under co-calcination or doping with H_3BO_3 were about 15.9 h, 23.4 h, 22.0 h and 24 h, respectively. Thus, regardless of the co-calcination or external mixing with boron in the free state, the addition of H_3BO_3 obviously delayed the hydration rate of the MOC by replacing the active MgO. As the reaction progressed, the concentration of the reactants continued to decrease, inhibiting the interaction between the MgO and $MgCl_2$ solution, thereby delaying the MOC hydration rate. The H_3BO_3 level replaced the active MgO, resulting in an obvious delay. As shown in Figure 4b, when the calcination temperature was 1000 °C, the control group T10 entered the acceleration phase for nearly 8.3 h. It was longer than that of the MOC prepared by calcination at 700 °C, which was attributed to the decrease in the activity of the MgO following the high-temperature calcination, and the rate of hydration

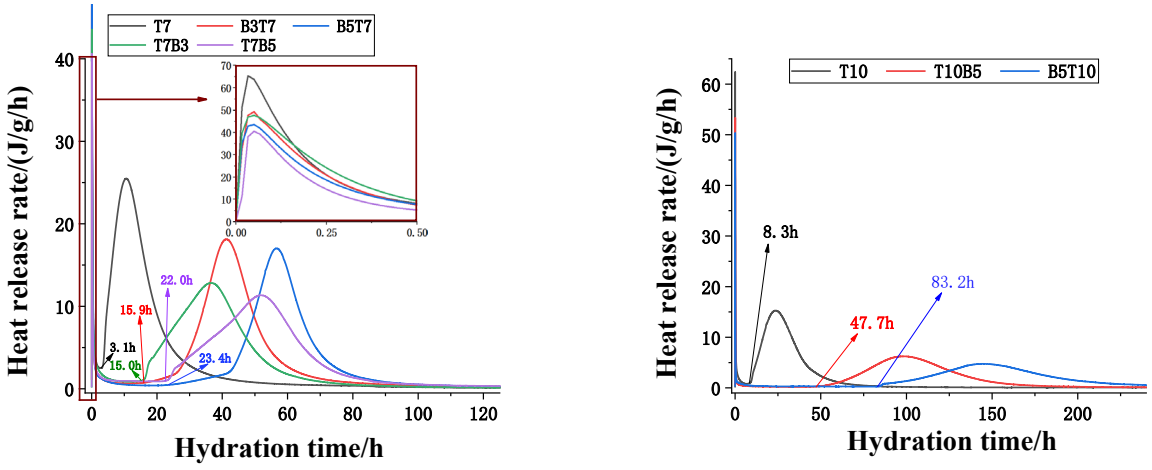

a) b)

Figure 4. Exothermic hydration rate of the MOC at the different temperatures and H_3BO_3 doping levels.

reaction with the $MgCl_2$ solution slowed down. After the addition of H_3BO_3, the start time of the acceleration period of T10B5 and B5T10 was about 47.7 h and 83.2 h, respectively, which further delayed the hydration rate of the MOC. The delaying effect due to co-calcination with boron was more obvious because, after calcination at high temperatures, a large amount of rough magnesium borate is generated and attached to the surface of MgO, resulting in a substantial delay in the hydration rate of the MOC. The result was also consistent with the law of compressive strength.

Hydration products and micromorphology

The hydration products and microscopic morphology of the MOC are key factors that determine the compressive strength of the MOC. The hydration products mainly include 5·1·8 crystals, which determine the strength of the MOC [16]. Figure 5 shows the XRD pattern of MOC after 1 and 28 days of curing with different doses of H_3BO_3 at 700 °C. As shown in Figure 5a, the stronger 5·1·8 phase diffraction peak in the control group T7 after 1 day of maintenance resulted in a higher MOC intensity than in the experimental group doped with H_3BO_3. The 1-d control group T7, which is the main hydration product of the MOC curing, in addition to the 5·1·8 phase, also contains a small amount of MgO, and the hydration products of B3T7, B5T7, T7B3, T7B5 after 1 day curing and doped with H_3BO_3 were also the 5·1·8 phases and MgO, indicating that the MOC hydration product remained unchanged by the co-calcination or doping with H_3BO_3. As shown in Figure 5b, when the 28-d MOC generated hydration products are all in the 5·1·8 phases, the hydration reaction resulted in the complete hydration of MgO without any residue. The diffraction peak of the 5·1·8 phase in the control group T10 was higher, so the intensity of the control group T10 was higher after 28-d maintenance.

As shown in Figure 6, the XRD spectrum of the 28-d MOC under different H_3BO_3 levels at 1000 °C reveals no condensation hardening at 1 day, so the XRD was not tested during 1 day of curing. After 28 days of MOC curing, the primary hydration product was 5·1·8. The diffraction peak of the 5·1·8 phase in the control group T10 was higher, whereas the diffraction peak of 5·1·8 in B5T10 was lower, suggesting that the T10 intensity was the highest after the 28-d maintenance and the B5T10 intensity was the lowest.

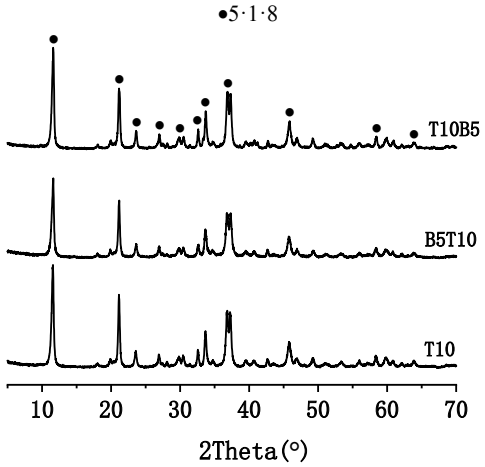

Figure 6. The XRD spectrum of the MOC after 28 days of curing under different H_3BO_3 levels at 1000 °C.

Figure 7 shows the SEM results of the MOC doped for 28-d with different levels of H_3BO_3 at 700 °C. Figure 7a shows that an extensive and large network of rod crystals was detected in the 5·1·8 phase, with a relatively dense structure. As shown in Figures 7b and

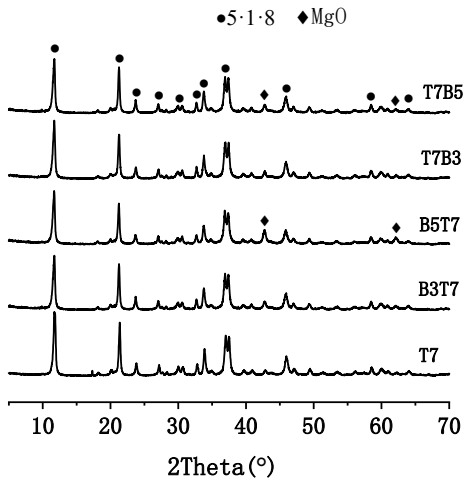

a)

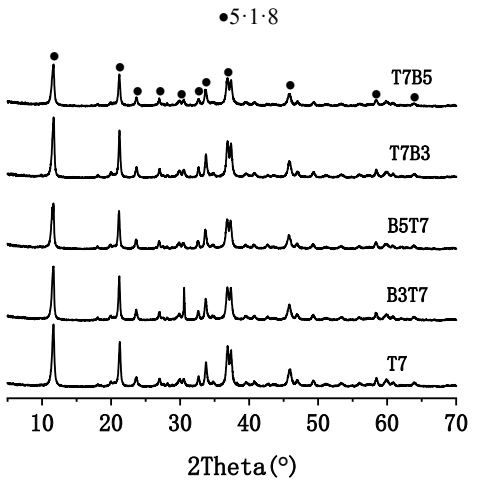

b)

Figure 5. XRD pattern of the MOC after 1 day and 28 days of curing with different H_3BO_3 doses at 700 °C.

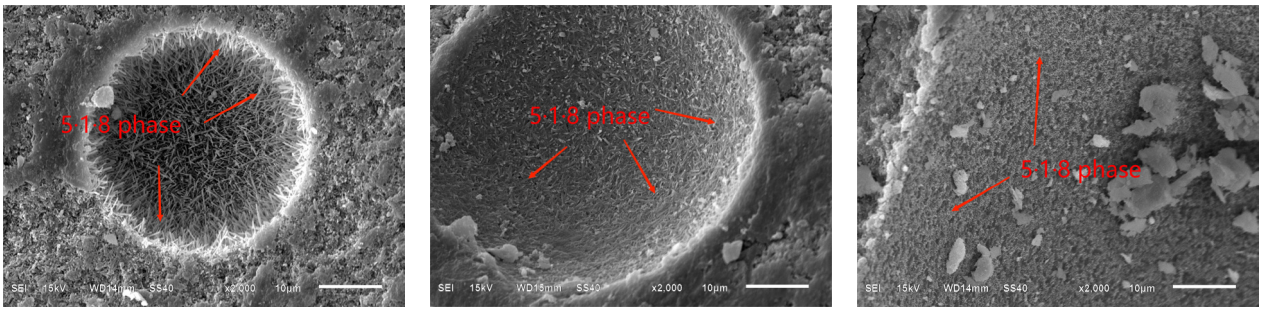

a) T7 b) B5T7 c) T7B5

Figure 7. SEM images of the MOC doped with H_3BO_3 for 28 days at 700 °C.

7c, the size of the 5·1·8 phase crystals in the MOC doped with boron impurities was substantially less than that of the control group, which corresponds to their intensity, suggesting that boron affects the crystal structure of the 5·1·8 phase and, in turn, alters the intensity.

Figure 8 shows the SEM image of the MOC doped with H_3BO_3 for 28-d at 1000 °C. As shown in the figure, the 5·1·8 phase distribution of the control group T10 was also dense, while the 5·1·8 phases in T10B5 and B5T10 were smaller in size and sparsely distributed. This result further shows that boron impurities affect the number and microscopic morphology of the 5·1·8 phase crystals, hindering their growth in each microscopic node of MOC. They decrease the number of 5·1·8 phase crystals and, thus, reduce the strength of the MOC.

Pore structure

The mechanical properties of cement depend on the type and content of the hydration products and are also closely related to the pore structure [17]. Figure 9 represents a comparative analysis of the cumulative porosity and differential pore size of the MOC cured for

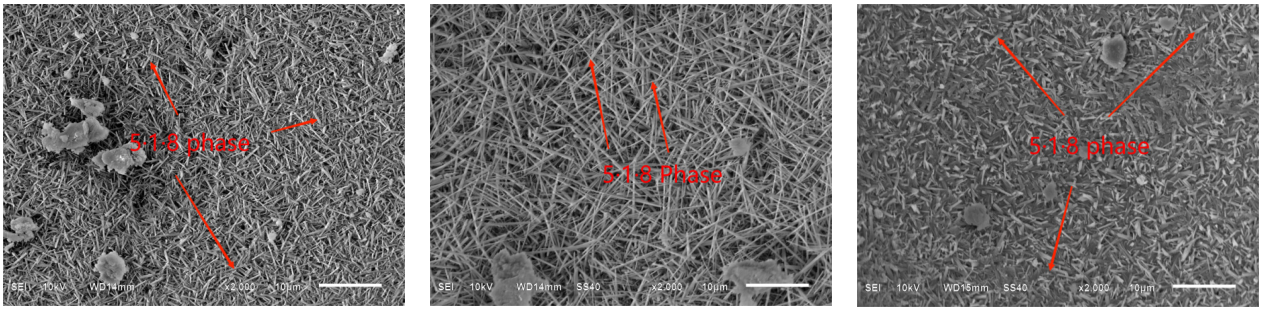

a) T10 b) B5T10 c) T10B5

Figure 8. SEM image of the MOCs doped with different doses of H_3BO_3 for 28 days at 1000 °C.

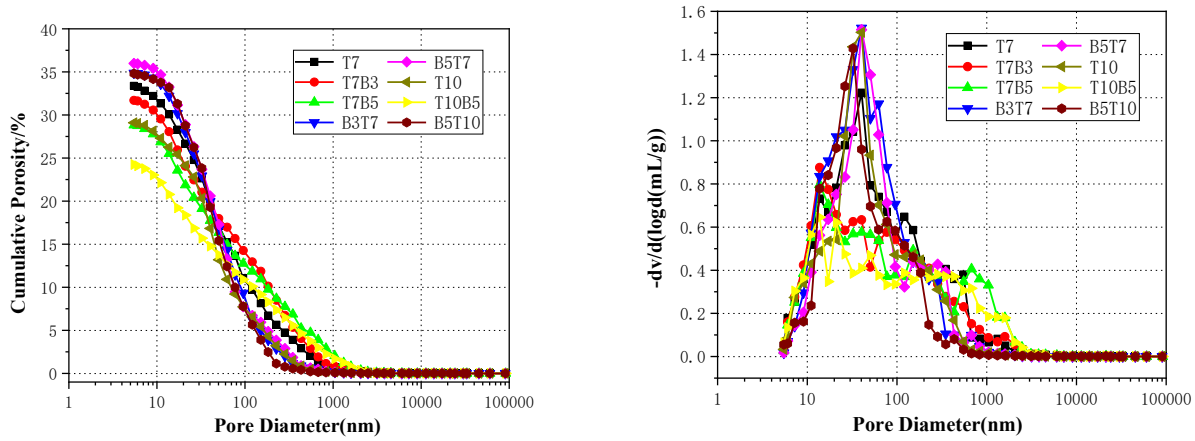

a) Cumulative porosity b) Differential pore size

Figure 9. MOC cured for 28 days at the different temperatures and dosages.

28-d at different temperatures and dosages. Calcination at 700 °C resulted in a 33.7 % porosity of the control group T7. In contrast, the porosity of the MOC was less than that of the control group T7 when co-calcined with 3 % and 5 % H_3BO_3, yielding a porosity of 31.69 % and 28.81 %, respectively. The addition of 3 % and 5 % H_3BO_3 enhanced the porosity of the MOC to 34.87 % and 35.98 %, respectively, compared with that of the control group. When the calcination temperature was 1000 °C, the porosity of the control group T10 was 29.09 % compared with the porosity of B5T10 (24.24 %) co-calcined with 5 % H_3BO_3. The porosity of T10B5 doped with 5 % H_3BO_3 was 34.82 %. Thus, the MOC prepared via calcination at low or high temperatures from the MgO precursor resulted in smaller sizes following co-calcination. A large amount of magnesium borate is generated during the co-calcination in which H_3BO_3 is attached to the surface of MgO and occupies the internal pores of the MOC, thereby reducing the MOC porosity. In contrast, the porosity of the MOC doped with $H_3BO_3$was greater than that of the control group, since H_3BO_3 and $Mg_2B_2O_5$ in the prepared MOC do not participate in the hydration reaction. The density of H_3BO_3 is 1.4 g·cm^{-3}, while the density of $Mg_2B_2O_5$ is 2.5 g·cm^{-3}; both are greater than the density of the 5·1·8 phase crystals (approximately 1.23 ~ 1.24 g·cm^{-3} [18]).

Table 5 shows the pore size distribution of the MOC. The pores of MOC are divided into gel pores (≤ 10 nm, beneficial pore size), small inter-grain pores (10 − 100 nm), and large inter-crystalline pores (≥ 100 nm, harmful pore size) [19]. As shown in Table 5, the MOC samples obtained via co-calcination with boron show a relatively large proportion of large inter-crystalline pores compared with the control group, while the MOC doped externally with boron constitute a relatively small proportion of gel pores. In addition, the average pore size of the control groups T7 and T10 was 16.46 nm and 29.79 nm, respectively. The average pore size increased after the addition of boron. The MOC showed obvious effects of external doping with free boron in terms of an increase in the average pore size of T7B5 and T10B5 by 244.35 % and 109.43 % to 56.68 nm and 62.39 nm, respectively, compared with the control group. This shows that the incorporation of a boron impurity changes the pore distribution of the MOC, increases the average pore size of the MOC, and thereby affects the performance of the MOC.

TG-DSC analysis of the results

Figure 10 shows the Thermogravimetry-differential scanning calorimetry (TG-DSC) curve after 28-d of MOC curing at the calcination temperatures of 700 °C and

Table 5. Pore size distribution of the MOC.

Samples	Porosity (%)	Average pore diameter (nm)	≤ 10nm (%)	10nm-100nm (%)	≥ 100nm (%)
T7	33.37	16.46	6.57	66.88	26.55
B3T7	31.69	25.36	6.68	55.11	38.21
B5T7	28.81	35.59	6.81	48.90	44.29
T7B3	34.87	40.16	4.63	75.08	20.29
T7B5	35.98	56.68	3.03	80.12	16.85
T10	29.09	29.79	6.18	60.41	33.41
B5T10	24.24	43.26	8.65	46.36	44.99
T10B5	34.82	62.39	3.08	74.98	21.94

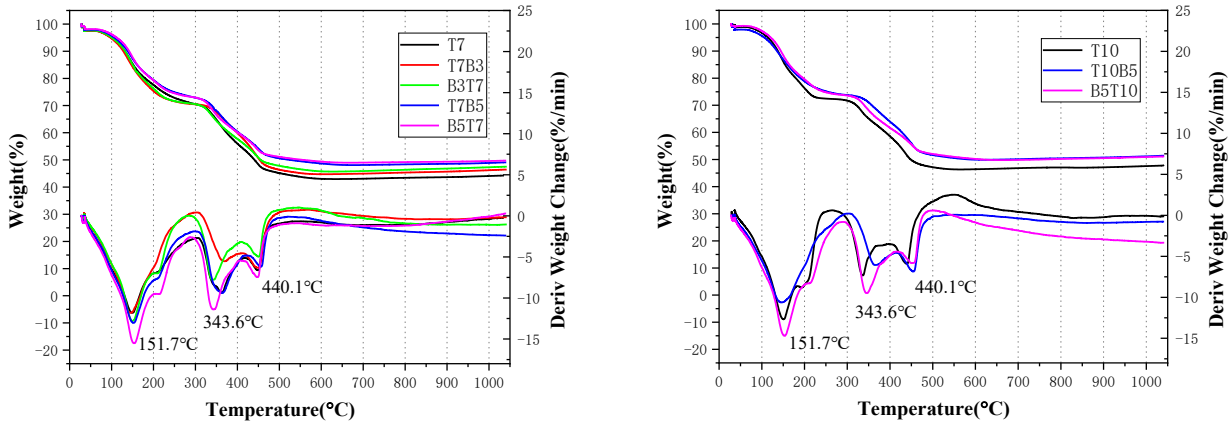

a) 700 °C

b) 1000 °C

Figure 10. Thermogravimetric curve of the MOC at the different calcination temperatures and dosages after curing for 28 days .

1000 °C. As shown in the figure, the DSC curve reveals three split heat absorption peaks at 151.7 °C, 343.6 °C, and 440.1 °C, respectively. The first endothermic peak corresponds to the decomposition of crystalline water in phase 5·1·8, during which 8 molecules of water of the crystallisation in the middle layer of the 5·1·8 phase are lost, resulting in an anhydrous phase ($5Mg(OH)_2 \cdot MgCl_2$). The second endothermic peak corresponds to the release of HCl gas during the heating of the MOC (Formula 4). Finally, the third endothermic peak is attributed to the decomposition of the remaining $Mg(OH)_2$ into MgO and water [20].

$$5Mg(OH)_2 \cdot MgCl_2 \rightarrow 4Mg(OH)_2 + 2MgO + 2HCl \quad (4)$$

In Figure 10, the DSC curve of the boron-containing impurity MOC significantly deviated from that of the control group. The co-calcined 5 % boric acid deviation was the largest and most obvious at the three endothermic peaks, indicating that the co-calcined boron sample decomposed the 5·1·8 phase, $5Mg(OH)_2 \cdot MgCl_2$, and $Mg(OH)_2$ needed to absorb more heat. This shows that boron impurities affected the microstructure of the 5·1·8 phase. As shown in the TG curve of Figure 10(a), the residual weights of T7, T7B3, B3T7, T7B5 and B5T7 were 44.24 %, 46.45 %, 47.51 %, 49.10 % and 49.75 %, respectively, suggesting a weight loss of 55.76 %, 53.55 %, 52.49 %, 50.90 % and 50.25 %, respectively. The TG curve of Figure 10b indicates that the residual weights of T10, T10B5 and B5T10 were 47.78 %, 48.64 % and 49.02 %, respectively, suggesting a loss of 52.22 %, 51.36 % and 50.98 %, respectively. The theoretical weight loss of 5·1·8 phase in the MOC is 56.16 % [20]. When the sample weight loss was closer to the theoretical value, the crystal content of the 5·1·8 phase was higher; however, the weight loss of the experimental groups doped with boron impurities were all lower than that of the control group. This indicated that relatively few of the 5·1·8 phase crystals decomposed in the samples doped with boron, which further verified that the higher the boron doping amount, the greater the impact on the MOC.

CONCLUSIONS

This study investigated the effect of boron impurities on the properties and mechanism of MOC. Based on the experimental results, the following conclusions are drawn:

(1) Boron impurities significantly impact the MOC due to their poor ionic binding with the $MgCl_2$ solution, which inhibited the formation of the 5·1·8 phase via the reaction of MgO with the solution. The effect of co-calcination with boron on the MOC is greater than that of the free form of boron, especially at high temperatures, indicating the obvious 'passivation' effect of the MgO during the co-calcination.

(2) The induction period during the hydration of the MOC prepared by co-calcining H_3BO_3 at 1000 °C was prolonged. Therefore, the MOC obtained via high-temperature calcination with boron-containing impurities and magnesium hydroxide is unsuitable for engineering applications. In addition, the findings suggest that MgO should be prepared at temperatures above 700 °C and below 900 °C because the MOC prepared below 700 °C cracked and warped easily, while the one obtained above 900 °C showed a loss in early strength of the cement.

(3) The existence of boron impurities affected the pore structure of the MOC, and the generation of 5·1·8 crystals, which impacted the performance of the MOC.

(4) In this study, the effects of boron impurities on the strength of the MOC in the magnesium by-product of the Salt Lake and their micro-mechanisms were studied. However, the presence of impurities such as Li, Na, and K in the raw materials (MgO and $MgCl_2$) generated by the MOC production from the Salt Lake Resources requires further investigation.

Acknowledgements

This study was supported by the National Natural Science Foundation of China (Grant No. 52002202) and The West Light Project of Chinese Academy of Sciences.

REFERENCES

1. Sorel S., (1867): On a new magnesium cement, C.R. Acad. Sci. 65 102–104.
2. Beaudoin J.J., Ramachandran V.S. (1975): Strength development in magnesium oxychloride and other cements. *Cement and Concrete Research, 5* (6) 617–630. doi: 10.1016/0008-8846(75)90062-9
3. Yu H. (1993). *Magnesium Oxychloride Cement and Its Application.* China Building Materials Industry Press, Beijing, China, 180-417.
4. Wu JY., Zhu SQ. (2019): The development of magnesium oxychloride cement and its products. *China Non-Met. Min. Ind. Her, 1*(3), 2006.
5. Li X., Zhang K., Shi R. (2017): Enhanced flame-retardant properties of cellulose fibers by incorporation of acid-resistant magnesium-oxide microcapsules. *Carbohydrate polymers, 176*, 246-256. doi: 10.1016/j.carbpol.2017.08.096
6. Huang Q., Li Y., Zheng W. (2020): Investigation on the properties of magnesium oxychloride cement prepared with seawater. *Advances in Cement Research, 32*(8), 379-388. doi: 10.1680/jadcr.18.00159
7. Bilinski H., Matkovic´ B., Mazuranic C. (1984): The formation of magnesium oxychloride phases in the systems $Mg\text{-}MgCl_2\text{-}H_2O$ and $NaOH\text{-}MgCl_2\text{-}H_2O$, *Journal of the American Ceramic Society, 67* (4) 266–269. doi: 10.1111/j.1151-2916.1984.tb18844.x
8. Dehua D., Chuanmei Z. (1999): The formation mechanism of the hydrate phases in magnesium oxychloride cemen. *Cement and Concrete Research, 29* (9) 1365-1371. doi: 10.1016/S0008-8846(98)00247-6
9. Wu Z., Li F. (2001): Development of magnesium chloride resources in salt lakes of Qinghai. *J. Salt Lake Res., 9*(2), 61-65.

10. Huang X., Zhang Q., Guo S., Wang G. (2004): The current situation and development prospects of magnesium resource utilization in China. Sea Lake Salt and Chemicals, 33(6), 1-6.
11. Haper F.C. (2013): Effects of calcinations temperature on properties of magnesium oxides for use in magnesium oxychloride cement. *Journal of Central South University, 20*(12), 3729-3735.
12. Yu J., Qian J., Wang F., Qin J., Dai X., You C., Jia X. (2020): Study of using dolomite ores as raw materials to produce magnesium phosphate cement. *Construction and Building Materials, 253*, 119147. doi: 10.1016/j.conbuildmat.2020.119147
13. Zheng W., Xiao X., Wen J., Chang C., An S., Dong, J. (2021): Water-to-cement ratio of magnesium oxychloride cement foam concrete with caustic dolomite powder. *Sustainability, 13*(5), 2429. doi: 10.3390/su13052429
14. Li Y., Dong J., Xiao X., Zheng W., Wen J., Chang C. (2020): Magnesium oxide and magnesium phosphate cement were prepared by using the sintering effect of common elements in salt lakes. *Salt Lake Studies, 28*(02),15-25.
15. Shi D., Zhang L., Peng X., Li L., Song F., Nie F., Ji L., Zhang Y. (2018): Extraction of lithium from salt lake brine containing boron using multistage centrifuge extractors. *Desalination, 441*, 44-51. doi: 10.1016/j.desal.2018.04.029
16. Ying L., Hongfa Y., Jinmei D. (2013): Research progress on hydration products, phase transition law and water-resistance evaluation method of magnesium oxychloride cement. *Acta Silicate Sinica, 41*(11), 1465-1473.
17. Wang F., Yang L., Guan L., Hu S. (2015): Microstructure and properties of cement foams prepared by magnesium oxychloride cement. *Journal of Wuhan University of Technology-Mater. Sci. Ed., 30*(2), 331-337. doi: 10.1007/s11595-015-1149-y
18. Guo Y., Zhang Y., Soe K., Pulham M. (2018): Recent development in magnesium oxychloride cement. *Structural Concrete, 19*(5), 1290-1300. doi: 10.1002/suco.201800077
19. Chen X., Zhang T., Bi W., Cheeseman C. (2019): Effect of tartaric acid and phosphoric acid on the water resistance of magnesium oxychloride (MOC) cement. *Construction and Building Materials, 213*, 528-536. doi: 10.1016/j.conbuildmat.2019.04.086
20. Jirickova A., Lojka M., Lauermannova A. M., Antoncík F., Sedmidubský D., Pavlikova M., Záleská M., Záleská M., Pavlík Z., Jankovský O. (2020): Synthesis, structure, and thermal stability of magnesium oxychloride $5Mg(OH)_2 \cdot MgCl_2 \cdot 8H_2O$. *Applied Science, 10*(5), 1683. doi:10.3390/app10051683